MNRAS **000**, 1–6 (2019) Preprint 20 February 2020 Compiled using MNRAS LATEX style file v3.0

The vanishing redshift as a probe of reionization

Kana Moriwaki,[1]★ Angus Beane,[2]† Adam Lidz,[3] and others
[1]*Department of Physics, The University of Tokyo, 7-3-1 Hongo, Bunkyo, Tokyo 113-0033, Japan*
[2]*Center for Astrophysics | Harvard & Smithsonian, 60 Garden Street, Cambridge, MA 02138, USA*
[3]*Department of Physics & Astronomy, University of Pennsylvania, 209 South 33rd Street, Philadelphia, PA 19104, USA*

Accepted XXX. Received YYY; in original form ZZZ

ABSTRACT
The early stages of the Epoch of Reionization (EoR), probed by the 21 cm line, are sensitive to the detailed formation of the first galaxies. An important transition occurs on large scales at $z \sim 10$, when the 21 cm field changes from being positively correlated with the density field to being negatively correlated. The redshift at which this occurs (the "vanishing redshift") is in principle measurable if the 21 cm field can be cross-correlated with a tracer of the density field (such as galaxies or a line intensity map) at that high redshift. Since the vanishing redshift is derived from a cross-correlation, it naively depends on the structure of the 21 cm field and the tracer field. However, we show that on large scales the transition redshift is independent of the structure of the tracer field. We verify this in simulations by assuming a simple model for a mock Lyα intensity mapping survey. By considering a joint measurement between the Square Kilometre Array and the Cosmic Dawn Intensity Mapper, we show that the vanishing redshift is measurable up until about $z \sim x$. Being derived from a cross-correlation, the vanishing redshift is less impacted by foreground contamination currently inhibiting 21 cm auto-spectrum measurements. Therefore, the vanishing redshift is an interesting probe of the early stages of the EoR, and its detectability and interpretability deserve further study.

Key words: cosmology: theory – dark ages, reionization, first stars – large-scale structure of Universe

1 INTRODUCTION

The redshifted 21 cm line contains a great deal of information about the structure and evolution of the Epoch of Reionization (EoR). Once measured at $z \sim 6$–12, it should reveal the nature of the formation of the first stars, galaxies, and black holes, as well as the large-scale structure of the Universe at high redshift (Loeb & Furlanetto 2013). While instruments have reached the sensitivity necessary to detect the signal during the EoR, issues of foreground contamination and instrumental artifacts have so far prevented the success of such efforts. Only upper limits have been placed on the amplitude of the 21 cm fluctuations (e.g. Paciga et al. 2013; Dillon et al. 2014; Beardsley et al. 2016; Patil et al. 2017).

Because of the difficulties in making 21 cm auto-spectrum measurements, the prospect of measuring 21 cm in cross-correlation with

Because of the great difficulties confronting 21 cm auto-spectrum measurements, the prospect of measuring 21 cm in cross-correlation with another tracer of large-scale structure, such as galaxies. The galaxy field will only correlate with the cosmological 21 cm signal, and the foregrounds will not contribute to the mean signal (though they will make the measurement noisy, and so some foreground subtraction is still necessary).

The 21 cm-galaxy cross-correlation was first explored by Wyithe & Loeb (2007) in the context of using Lyα-emitters to distinguish between "inside-out" and "outside-in" reionization scenarios. However, this technique is limited to the late stages of reionization since Lyα-emitters are obscured by neutral hydrogen even slightly earlier into the EoR (e.g. Kashikawa et al. 2006). Furlanetto & Lidz (2007) expanded upon this by considering a general galaxy survey. It was later shown that the scale at which the cross-correlation goes from negative to zero (the "turnover scale") provides a tracer of the bubble size. However, the precise turnover scale also depends on the properties of the selected galaxy sample, with turnover happening on larger scales if only more massive galaxies can be detected (Lidz et al. 2009). A number of authors have studied this cross-correlation in the context of detectability of the anti-correlation on large scales (Wiersma et al. 2013; Vrbanec et al. 2016; Hutter et al. 2017), and its dependence on the details of the EoR (Park et al. 2014).

In addition to the cross-correlation between 21 cm and galaxies, the cross-correlation between 21 cm and intensity maps has been investigated in an analogous fashion. Line intensity mapping experiments aim to measure the large-scale structure of emission in a certain line, and is easier to perform over a large area at high redshift than a galaxy survey. Current targets include [C II], CO,

★ E-mail: kana.moriwaki@utap.phys.s.u-tokyo.ac.jp
† E-mail: angus.beane@cfa.harvard.edu

Lyα, and Hα (for a recent review, see Kovetz et al. 2017). Another intriguing possible line is [O III] 88 μm (e.g. Moriwaki et al. 2018), in which a lensed $z = 9.1$ galaxy has recently shown to be exceptionally bright (Hashimoto et al. 2018).

This cross-correlation was first studied with the CO rotational lines (Lidz et al. 2011), and then the [C II] (Gong et al. 2012) and Lyα lines (Silva et al. 2013). The possibility of using the cross-bispectrum the 21 cm and [C II] fields has been explored (Beane & Lidz 2018), along with combining the three cross-spectra with a 21 cm, [C II], and [O III] overlap (Beane et al. 2019). Because the vanishing redshift is typically $z_v \sim 10$, it is unclear how much metal enrichment will have occurred by this early time.

In the case of either galaxies or emission lines, it is expected that the two are positively correlated at the very beginning of the EoR (though the emission lines may be very weak due to the lack of significant metal enhancement). This is because the densest regions host the most mass and therefore 21 cm emission and galaxy populations. However, the densest regions will also ionize first **cite something**, and after some time 21 cm and galaxies will become negatively correlated. We refer to the redshift at which this transition occurs at a fixed k as the "vanishing redshift" $z_v(k)$, assuming that only one such zero exists. In other words, the cross-correlation at k vanishes at $z = z_v(k)$.

In this work we investigate to what extent the vanishing redshift is dependent upon the galaxy sample used to define it. We assume a galaxy catalog selected using an [O III] emitter survey. In particular, we are interested in how z_v changes as we vary the parameters of the [O III] luminosity-mass relation for a fixed halo catalog.

2 METHODS

2.1 The vanishing redshift

The vanishing redshift $z_v(k)$ is defined by a field x which traces the density field on large scales and the condition that

$$P_{21,x}(k, z_v(k)) \equiv 0. \quad (1)$$

If more than one such z_v exists, then we choose the lowest one where $P_{21,x}$ last transitioned from positive to negative.

2.2 21cmFAST

We generate realizations of the 21 cm field for our different EoR models using the publicly available code `21cmFAST` v1.3[1]. Spin temperature fluctuations are computed and the excursion set approach is used to identify the ionized regions (Mesinger et al. 2011). Rather than using the mean collapsed fraction, we use the halo field to compute the ionization and 21 cm fields, since we are interested in the evolution at early redshifts where the Poisson statistics of the halo field can be important.

The parameters used in our `21cmFAST` runs are as folows. The minimum halo mass contributing to the ionizing budget is $10^8\,\mathrm{M}_\odot$. The H II efficiency factor (ζ) is set to 10. The maximum smoothing scale for the ionization field R_{max} (loosely referred to as the "mean-free path") is set to 30 Mpc, though this quantity has almost no effect on the early stage of the EoR. We set the fraction of baryons converted to stars ($f_\star$) to be 0.1. We ignore redshift-space distortions for convenience. All other parameters are set to their default values, except for the heating parameter discussed in the next paragraph. The exact parameter files are given in the github repository associated with this work (see the Supplementary Material).

Our three different models for the EoR differ in the efficiency of their heating, controlled by the number of X-ray photons per solar mass in galaxies (ζ_X). Our fiducial model (`fid`) is the default value $\zeta_X = 2 \times 10^{56}$, while our "hot" and "cold" models (`hot` and `cold`) set $\zeta_X = 10^{57}$ and 5×10^{55}, respectively. The average δT_b signal is shown in **some figure**, which shows **something**. Note that none of these models account for the recent claimed detection by the EDGES group of an extremely deep absorption trough at $z \sim 17$ (Bowman et al. 2018). If confirmed, though, that detection would indicate an extremely low gas temperature at $z \sim 17$, which would favor larger amplitudes of the spin temperature fluctuations at $z \sim 10$, unless heating were extremely efficient after $z \sim 17$. **don't know how I feel about the last sentence**

We generate the halo field using the included halo finder in `21cmFAST`. This halo finder is a remnant of an earlier version of the code (Mesinger & Furlanetto 2007) and is typically unused in standard configurations. It is based upon the "peak-patch" algorithm for halo finding introduced by Bond & Myers (1996).

2.3 Intensity mapping

In order to model the relation between luminosity (L) and halo mass, we follow Beane et al. (2019). Specifically, we assume that the mean luminosity of a halo of mass M is,

$$\langle L \rangle (M) = L_0 \left[\frac{M}{M_0} \right]^\alpha , \quad (2)$$

where L_0/M_0^α is set to match the total average intensity of the line at that redshift and α is the power-law index. We then draw the luminosity of each halo from a lognormal distribution of mean $\langle L \rangle (M)$ and scatter σ. Once the average intensity is fixed (which we assume so), this is a two-parameter model (α and σ) of the luminosity-mass relation. In practice, the average intensity of the field only enters in the detectability calculation, so we instead work in the convenient units where $L_0 = 1$ and $M_0 = 10^{10}\,\mathrm{M}_\odot$.

We assign a luminosity to each halo according to this prescription. An important consideration is that we have not specified which line we are working with. In detail, the relationship between a halo and it's luminosity is a complicated function of the state of the interstellar medium of the hosted galaxy, which can depend upon a number of both deterministic and stochastic quantities. Our model crudely attempts to account for this by including some random scatter, but will ultimately be a rough description of reality.

Some words justifying why our simple model will extend to more complicated luminosity-halo relations.

3 RESULTS

3.1 The vanishing redshift

3.2 The halo field

If we switch to LIM I think this section should be scrapped, except showing ztran vs k but using LIM and density instead of halos

We first investigate the dependence of the vanishing redshift as defined by the halo field. Fig. 2 shows the vanishing redshift defined by the 21 cm – density cross-power spectrum (see Eq. 1) as

[1] https://github.com/andreimesinger/21cmFAST, commit: 42e7566

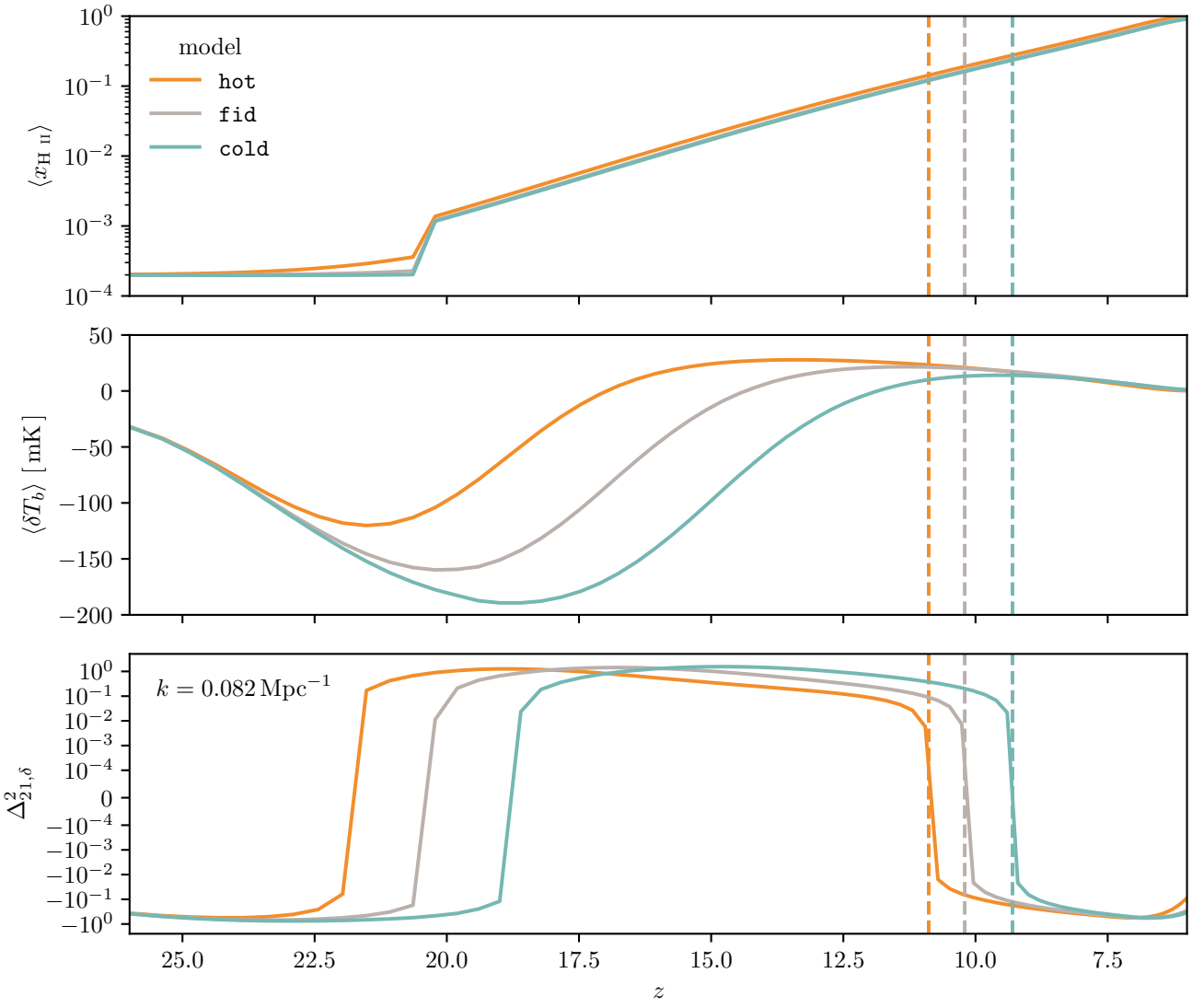

Figure 1. A summary of the ionization and heating history of our three EoR models: `hot`, `fid`, and `cold`. *Upper*: the ionization history of each model, showing that reionization begins ($\langle x_{\rm H\,II}\rangle \sim 0.01$) at $z \sim 16$ and ends at $z \sim 6$ in each model. In detail the ionization histories are slightly different, but not drastically. *Lower*: the heating history of each model, showing the strong differences in the monopole signal. The vanishing redshift z_ν (defined where $P_{21,\delta}(z_\nu) = 0$) for each model is shown as a vertically dashed line. We see that models in which heating is more efficient have an earlier z_ν.

a function of k. The three models considered in this work are shown in orange, gray, and teal (`hot`, `fid`, and `cold`, respectively).

Fig. 2 shows that z_ν is only weakly a function of k.

3.3 Line-intensity mapping

We now turn to understanding how z_ν depends on the parameters of our generic line-intensity mapping field: the slope (α) and lognormal scatter (σ). See § 2.3 for more details of the construction of the field.

In Fig. 4 we plot z_ν as a function of each of these parameters – α and σ. We see that z_ν is remarkably insensitive to the value of either of these parameters, with some small deviation as a function of α. The `hot`, `fid`, and `cold` models only vary by a total of 1.2%, 0.56%, 0.52% with respect to α, and 0.070%, 0.10%, and 0.11% with respect to σ, respectively.

4 DETECTABILITY

Up to this point, we have not been specific about which galactic emission line one might consider using to measure z_ν – in fact, our entire formalism could be executed using a galaxy survey, if one with sufficient redshift accuracy and depth could be executed. While it will not be possible for a traditional galaxy survey to extend to $z \sim 10$ in the near future, it may be possible to execute a survey of line-emitting galaxies, e.g., with [O III]-emitters (Moriwaki et al. 2018, 2019).

In this work we will consider the prospect of performing intensity mapping measurements of the Hα line using the proposed, space-based Cosmic Dawn Intensity Mapper (CDIM) (Cooray et al. 2019). CDIM is an infrared telescope with an 83 cm dish capable of measuring $R = 300$ spectra from wavelengths 0.75 μm to 7.5 μm. Therefore, CDIM will be able to measure the H-α line (656 nm)

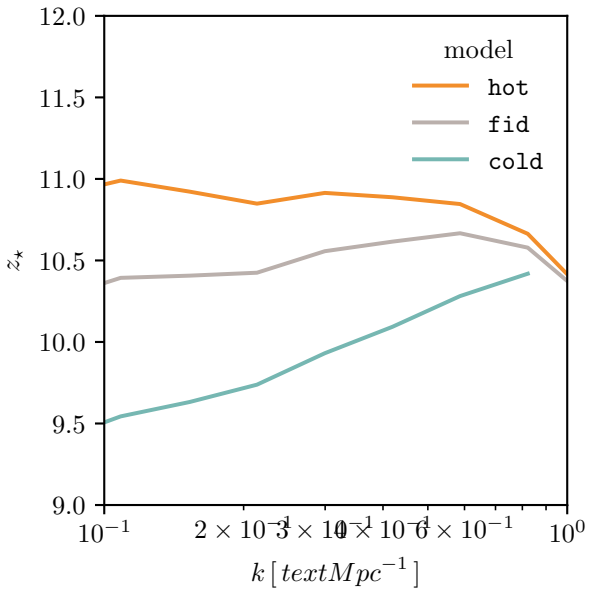

Figure 2. The vanishing redshift (z_v) as defined by cross-correlating with the density field (solid lines) and all resolved halos (dashed lines, $M \gtrsim 5 \times 10^9\,\mathrm{M}_\odot$), for our three different EoR models (`hot`, `fid`, and `cold`). We see that z_v is only a mild function of k for the three models, with slightly stronger dependence as the heating of the model decreases. The most dependence comes in the `cold` model, where z_v changes by $\sim 7\,\%$ from $k = 0.1$ to $0.6\,h\,\mathrm{Mpc}^{-1}$. **Some words for why cold and fid cut off at some k**

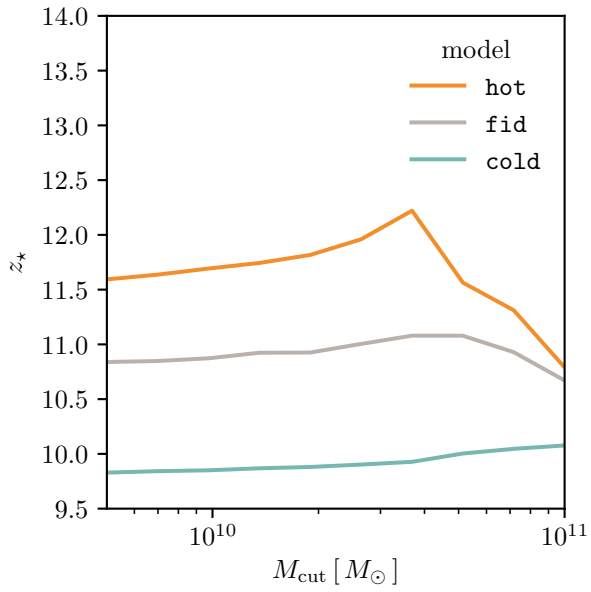

Figure 3. The vanishing redshift (z_v) as defined by cross-correlating with the halo field for our three different EoR models (`hot`, `fid`, and `cold`) as a function of the cut-off mass. The cross-correlation is only made between the 21 cm field and all halos with masses $M > M_{\rm cut}$. One can see that for the `fid` and `cold` models, z_v is only mildly a function of $M_{\rm cut}$ below a certain cut-off mass ($\sim 10^{10.5}\,\mathrm{M}_\odot$ in both models). In other words, as long as a galaxy survey is deep enough so as to resolve a sufficient number of galaxies, the z_v is not dependent on the depth of the survey. The `hot` model shows more dependence, but this may be due to sampling noise due to the smaller number of such halos at the higher z_v typical for the `hot` model.

from $z = 0.14$ to 10.4 and the H-β line (486 nm) from $z = 0.54$ to 14.4, so long as there is a detectable signal. CDIM will execute a wide, medium, and deep survey of 311, 31.1, and 15.6 deg^2, respectively. However, only the medium survey's field will overlap with 21 cm experiments (HERA and a deep field from SKA1-LOW). Therefore we will only consider the medium survey.

We choose to study the H-α and H-β lines since the uncertainty regarding their total intensity at $z \sim 10$ should be less uncertain than for lines that require metal enrichment such as [C II], [O III], or [N II], since the total metal enrichment of the universe is quickly declining at these high z

We assume a linear relationship between H-α luminosity and star formation rate (Kennicutt 1998):

$$\begin{aligned} L_{\mathrm{H}\alpha} &= 3.29 \times 10^7 \left(\frac{\mathrm{SFR}}{1\,\mathrm{M}_\odot\,\mathrm{yr}^{-1}}\right) L_\odot \\ &\equiv L_{0,\mathrm{H}\alpha} \left(\frac{\mathrm{SFR}}{1\,\mathrm{M}_\odot\,\mathrm{yr}^{-1}}\right) \end{aligned} \tag{3}$$

This relation is based on a Salpeter IMF and is calibrated towards local galaxies. As discussed in Katz et al. (2019), the reality of $z \sim 10$ galaxies may be slightly different – the IMF may be more top heavy, and the metal-poor nature of a typical star will naturally produce more ionizing photons. However, the escape of ionizing photons may be more efficient at higher redshift, and the conventional relation assumes no escape. Katz et al. (2019) provide a slightly shallower fitting form for the $L_{\mathrm{H}\alpha}$ − SFR relation based upon their simulations, but we choose to use the conventional relation here.

We use a fitting formula for the SFRd calibrated upon galaxies from $z = 0$ to 8 (Madau & Dickinson 2014)

$$\psi(z) = 0.015 \frac{(1+z)^{2.7}}{1 + [(1+z)/2.9]^{5.6}}\, M_\odot \mathrm{yr}^{-1} \mathrm{Mpc}^{-3}. \tag{4}$$

The comoving emissitivity of the Hα line can then be readily computed as,

$$\epsilon_{\mathrm{H}\alpha}(z) = L_{0,\mathrm{H}\alpha}\psi(z). \tag{5}$$

The average specific intensity can be computed from the comoving emissitivity as (Lidz et al. 2011; Pullen et al. 2013),

$$\langle I_{\mathrm{H}\alpha}\rangle(z) = \frac{\epsilon_{\mathrm{H}\alpha}(z)}{4\pi\nu_{\mathrm{rest,H}\alpha}} \frac{c}{H(z)} \tag{6}$$

The variance per mode of the cross-spectrum between the 21 cm field and a line i is given by (e.g. Furlanetto & Lidz 2007)

$$\mathrm{Var}[P_{21,i}] = P_{21,i}^2 + P_{21,\mathrm{tot}} P_{i,\mathrm{tot}}, \tag{7}$$

where $P_{21,\mathrm{tot}} = P_{21,21} + N_{21}$, where N_{21} is the total noise contribution. $P_{i,\mathrm{tot}}$ is defined similarly.

In detail the surface brightness sensitivity will have a frequency-dependent structure, but for $z \sim 9$ to 10, it is reasonable to assume a conservative, constant value of $\sigma_{\mathrm{H}\alpha} \sim 4 \times 10^4$ Jy/sr for the medium survey. To convert the surface brightness sensitivity to a power spectrum noise, we simply write,

$$N_{\mathrm{H}\alpha} = \sigma_{\mathrm{H}\alpha}^2 V_{\mathrm{voxel}}, \tag{8}$$

where V_{voxel} is the comoving volume of one voxel. To compute this

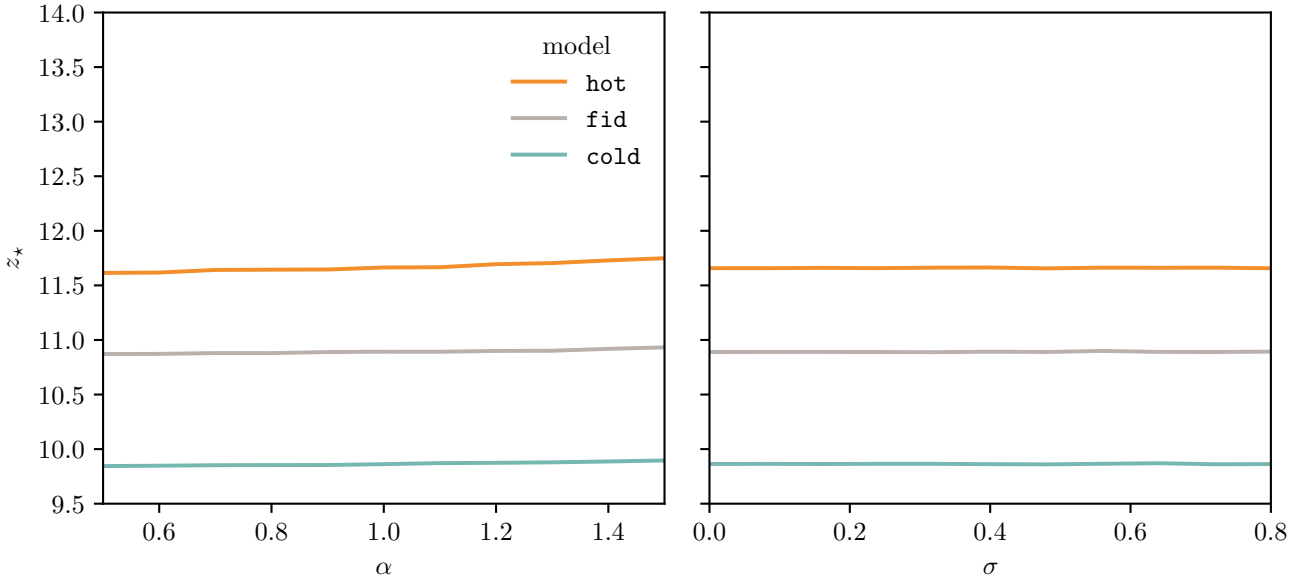

Figure 4. The vanishing redshift (z_ν) defined by cross-correlating with a generic two-parameter intensity mapping field. The parameter α sets the slope of the luminosity-mass relation and the parameter σ sets the lognormal scatter in this relation (see § 2.3). The `hot`, `fid`, and `cold` models only vary by a total of 1.2%, 0.56%, 0.52% with respect to α, and 0.070%, 0.10%, and 0.11% with respect to σ, respectively. Clearly z_ν varies only with the structure of the 21 cm field, and is thus an excellent probe of reionization.

we use the fact that CDIM will have $1''$ pixels and a resolution of $R = 300$.

For N_{21}, we assume that $N_{21} = P_{21,21}(k = 0.1\,\mathrm{Mpc}^{-1})$, a reasonable approximation given that HERA-350 will image some large scale modes (DeBoer et al. 2017), as discussed previously (Beane & Lidz 2018).

The number of modes is given by,

$$N_m = \frac{4\pi k^2 \delta k}{V_{\rm fund}}, \tag{9}$$

where δk is the width of the k-bin and $V_{\rm fund}$ is the volume of a fundamental mode. We assume a square survey area, and so this is given by,

$$V_{\rm fund} = \frac{(2\pi)^3}{L_\perp^2 L_\parallel}, \tag{10}$$

where $L_\perp$ is the and $L_\parallel$ is the comoving length of the redshift extent of the bin. The optimal redshift binning is not entirely clear, since the observational target is not the power spectrum. We assume a redshift bin of $\Delta z = 0.03$, which is smaller than the expected error we compute on z_ν, and so is not an unreasonable choice. We assume a k-bin of fairly large width, from $k = 0.1$ to $0.4\,\mathrm{Mpc}^{-1}$.

By expanding $P_{21,\mathrm{H}\alpha}$ as a linear function about z_ν, we can estimate the error on z_ν by

$$\mathrm{Var}[z_\nu] = \left(\frac{\partial P_{21,\mathrm{H}\alpha}}{\partial z}\bigg|_{z_\nu} \right)^{-2} \mathrm{Var}[P_{21,\mathrm{H}\alpha}], \tag{11}$$

where $\partial P_{21,\mathrm{H}\alpha}/\partial z$ is computed numerically.

5 CONCLUSIONS

The conclusions.

ACKNOWLEDGEMENTS

The Acknowledgements section.

UTILITY

Some links to be saved for later

Lyα intensity L_0 source: https://iopscience.iop.org/article/10.1088/0004-637X/743/1/65/meta

REFERENCES

Beane A., Lidz A., 2018, ApJ, 867, 26
Beane A., Villaescusa-Navarro F., Lidz A., 2019, ApJ, 874, 133
Beardsley A. P., et al., 2016, ApJ, 833, 102
Bond J. R., Myers S. T., 1996, ApJS, 103, 1
Bowman J. D., Rogers A. E. E., Monsalve R. A., Mozdzen T. J., Mahesh N., 2018, Nature, 555, 67
Cooray A., et al., 2019, arXiv e-prints, p. arXiv:1903.03144
DeBoer D. R., et al., 2017, PASP, 129, 045001
Dillon J. S., et al., 2014, Phys. Rev. D, 89, 023002
Furlanetto S. R., Lidz A., 2007, ApJ, 660, 1030
Gong Y., Cooray A., Silva M., Santos M. G., Bock J., Bradford C. M., Zemcov M., 2012, ApJ, 745, 49
Hashimoto T., et al., 2018, Nature, 557, 392
Hutter A., Dayal P., Müller V., Trott C. M., 2017, ApJ, 836, 176
Kashikawa N., et al., 2006, ApJ, 648, 7
Katz H., et al., 2019, MNRAS, 487, 5902
Kennicutt Robert C. J., 1998, ARA&A, 36, 189
Kovetz E. D., et al., 2017, arXiv e-prints, p. arXiv:1709.09066
Lidz A., Zahn O., Furlanetto S. R., McQuinn M., Hernquist L., Zaldarriaga M., 2009, ApJ, 690, 252

Lidz A., Furlanetto S. R., Oh S. P., Aguirre J., Chang T.-C., Doré O., Pritchard J. R., 2011, ApJ, 741, 70
Loeb A., Furlanetto S. R., 2013, The First Galaxies in the Universe
Madau P., Dickinson M., 2014, ARA&A, 52, 415
Mesinger A., Furlanetto S., 2007, ApJ, 669, 663
Mesinger A., Furlanetto S., Cen R., 2011, MNRAS, 411, 955
Moriwaki K., et al., 2018, MNRAS, 481, L84
Moriwaki K., Yoshida N., Eide M. B., Ciardi B., 2019, arXiv e-prints, p. arXiv:1906.10863
Paciga G., et al., 2013, MNRAS, 433, 639
Park J., Kim H.-S., Wyithe J. S. B., Lacey C. G., 2014, MNRAS, 438, 2474
Patil A. H., et al., 2017, ApJ, 838, 65
Pullen A. R., Chang T.-C., Doré O., Lidz A., 2013, ApJ, 768, 15
Silva M. B., Santos M. G., Gong Y., Cooray A., Bock J., 2013, ApJ, 763, 132
Vrbanec D., et al., 2016, MNRAS, 457, 666
Wiersma R. P. C., et al., 2013, MNRAS, 432, 2615
Wyithe J. S. B., Loeb A., 2007, MNRAS, 375, 1034

APPENDIX A: SOME EXTRA MATERIAL

The appendix.

This paper has been typeset from a TEX/LATEX file prepared by the author.